

FIP-GNN: Graph neural networks for scalable prediction of grain-level fatigue indicator parameters

Gyu-Jang Sim^a, Myoung-Gyu Lee^a, Marat I. Latypov^{b,c,*}

^aDepartment of Materials Science and Engineering & RIAM, Seoul National University, 1 Gwanak-ro, Gwanak-gu, Seoul 08826, Korea

^bDepartment of Materials Science and Engineering, University of Arizona, Tucson, AZ 85721, USA

^cGraduate Interdisciplinary Program in Applied Mathematics, University of Arizona, Tucson, AZ 85721, USA

Abstract

High-cycle fatigue is a critical performance metric of structural alloys for many applications. The high cost, time, and labor involved in experimental fatigue testing call for efficient and accurate computer models of fatigue life. We present FIP-GNN – a graph neural network for polycrystals that (i) predicts fatigue indicator parameters as grain-level inelastic responses to cyclic loading quantifying the local driving force for crack initiation and (ii) generalizes these predictions to large microstructure volume elements with grain populations well beyond those used in training. These advances can make significant contributions to statistically rigorous and computationally efficient modeling of high-cycle fatigue – a long-standing challenge in the field.

Note: **this is an author-generated postprint** of the article by Sim et al. [published](#) in *Scripta Mater.* (2025). DOI: 10.1016/j.scriptamat.2024.116407

Keywords: Graph neural networks, High-cycle fatigue, Fatigue indicator parameters, Microstructure

Understanding and predicting fatigue are crucial in designing and qualifying structural alloys. Determining alloy lifespan in high cycle fatigue (HCF) is challenging due to its variability [1] and the time-consuming cycling tests needed for crack initiation. The cost, time, and labor of experimental HCF testing highlight the need for efficient and accurate models.

One approach to modeling HCF aims to compute the driving force for crack initiation as crack initiation accounts for most of the HCF life in polycrystalline alloys [2]. The driving force is often quantified by a fatigue indicator parameter (FIP) calculated in microstructure-based simulations, e.g., crystal plasticity finite element (CPFE) method [3]. Calculation of FIPs that best predict crack initiation has been subject to intensive research [4], leading to the introduction of various FIPs [3, 5–8]. The

Fatemi–Socie FIP is widely used due to its low mesh sensitivity [9] and its accessibility within continuum CPFE simulations without explicit crack tip implementation. Utilizing the Fatemi–Socie FIP as a metric of the driving force for crack initiation, Przybyla et al. [10] developed a methodology of evaluating and ranking microstructures in terms of their HCF resistance. Their approach uses statistical analysis of FIP values in polycrystalline microstructure volume elements (MVEs). However, the method faces challenges because statistical analysis of most interest for the HCF resistance focuses on extreme value (EV) distributions that require MVEs prohibitively large for CPFE simulations. For an Al 7075-T6 alloy, MVEs containing even 10^6 grains were reported insufficiently representative for FIP EV distributions, which is already impractically expensive – a CPFE simulation on one MVE with only 1000 grains requires over 100 CPU hours [11]. Given the high computational cost and the need in large grain populations for EV distributions, researchers adopted the con-

*corresponding author

Email address: latmarat@arizona.edu (Marat I. Latypov)

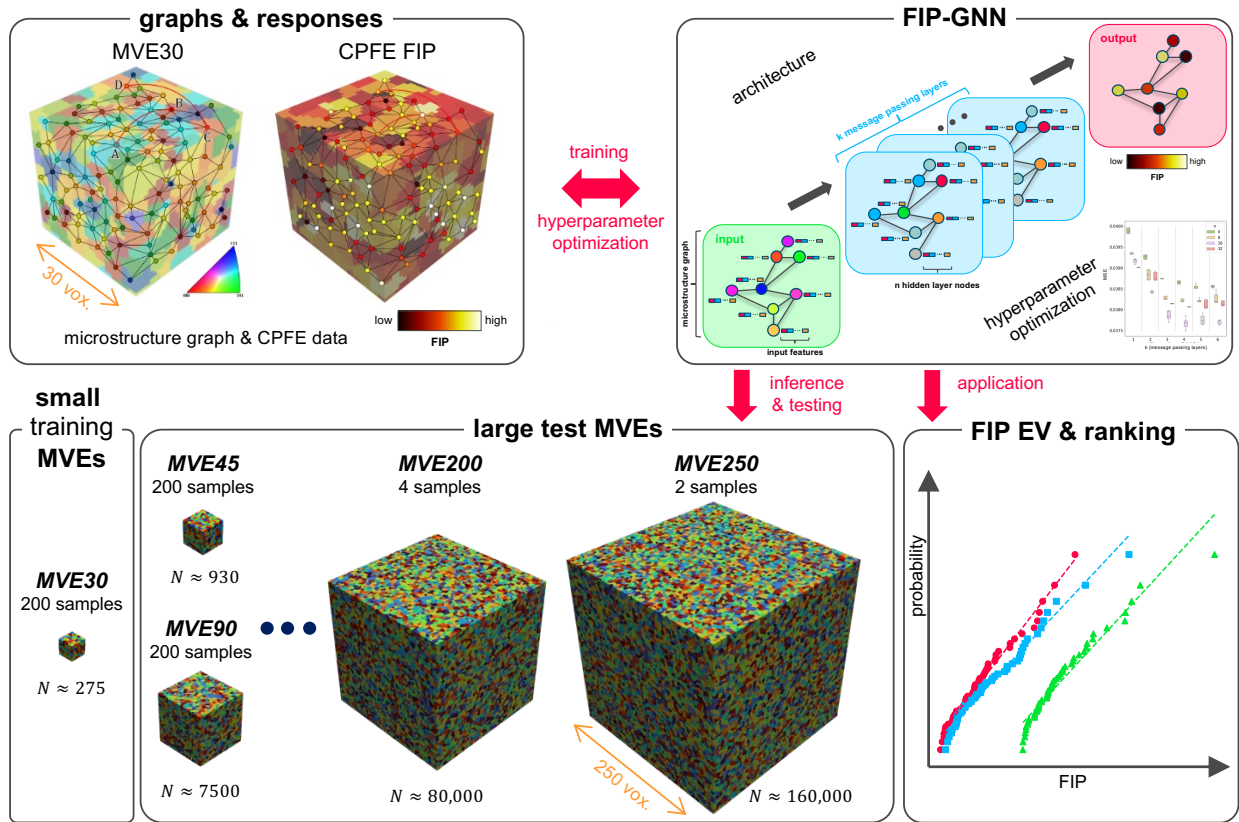


Figure 1: Pictorial overview of this study, including training and optimization of GNNs with small MVEs (MVE30 set), GNN architecture, large MVEs used for testing the predictive capabilities of GNNs for modeling grain-level FIPs, and predicting FIP EV distributions as the application for trained GNNs. MVE sets (MVE30, MVE45, . . . , MVE250) are labeled according to the number of voxels (“vox.”) along one side of the cube MVEs. Only one example MVE is visualized for each set, total number of MVEs (“samples”) and approximate number of grains, N , for each MVE size are also provided.

cept of statistical volume elements (SVEs), where multiple volume elements represent one microstructure in lieu of one large MVE [12–14]. SVEs allow estimating FIP EV distributions from large grain populations in aggregate, though it is still computationally expensive due to the need in CPFE simulations on multiple volume elements for each microstructure.

The high computational cost of the CPFE method for statistically rigorous modeling of HCF emphasizes the need in new efficient approaches. Machine learning is a promising route for reducing the computational cost of modeling microstructure–property relationships. A machine learning strategy extensively explored in literature is the development of surrogate models that reproduce the results of computationally demanding direct numerical simulations such as CPFE at a fraction of their computational cost. Quite a few surrogate models

have been reported to date [14–31].

The surrogate models primarily differ in their approach to quantitative description of microstructure. Reported descriptions include spatial correlations [14–16], latent representation by convolutional neural networks learned during training [17, 18, 32, 33], and graphs [19–29]. Graph representation of polycrystals and use of graph neural networks (GNNs) have been gaining momentum, as graphs capture grain structure and connectivity in polycrystals without requiring full 3D voxel data unlike other descriptions. GNNs have been successful in modeling various properties of polycrystals, both mechanical [19–25, 29] and non-mechanical [26–28]. Vlassis et al. [19] developed GNN models to predict the elastic energy in hyperelastic materials. Pagan et al. [20] trained GNNs to predict grain-average stress in Ni and Ti alloys using CPFE and experimental data. Sadeghpour

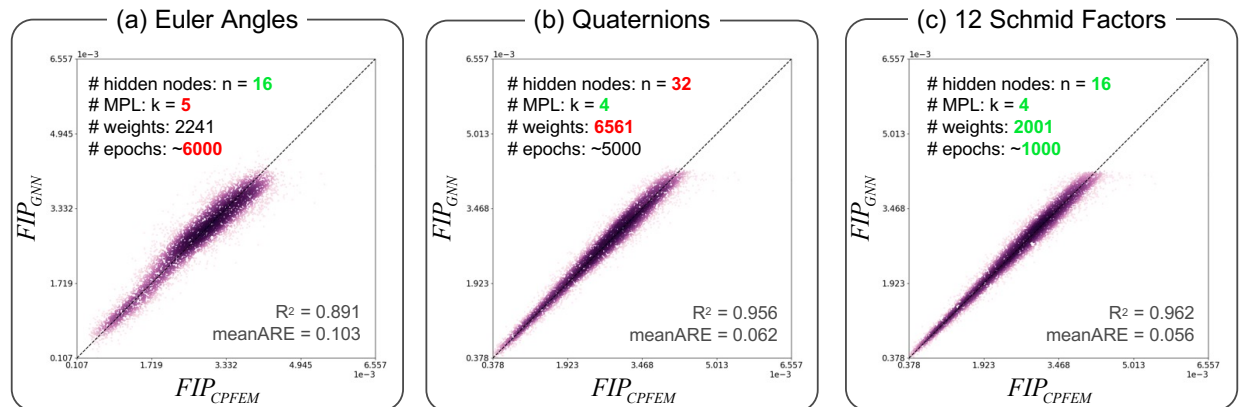


Figure 2: Parity plots comparing grain-level FIPs predicted by the GNN vs. those from CPFE simulations for 20 microstructures from the MVE30-VAL set. The parity plots are shown for three GNNs with optimized hyperparameters (n and k) based on (a) Euler angles, (b) quaternions, (c) 12 Schmid factors as graph node features. The corresponding MeanARE and R^2 as well as the number of learnable weights and number of epochs to reach a plateau in the validation loss are also shown.

et al. [21] modeled the yield strength of 316L steel, while Hestroffer et al. [22] developed GNNs for the yield strength and elastic modulus of α -Ti. Hu and Latypov [25] generalized GNNs ability to predict anisotropic properties in arbitrary loading directions. Thomas et al. [23] developed GNNs to predict fatigue based on experimental data on surface protrusions. Hu et al. [29] combined a GNN with recurrent neural networks to predict grain orientation and stress history in polycrystals. These studies demonstrated the potential of GNNs for modeling overall properties and grain-level responses in polycrystals and render GNNs promising for computationally efficient FIP prediction. While machine learning of FIPs have been recently pursued – e.g., Hansen et al. [30] used symbolic regression for learning interpretable dependence of FIPs on microstructure; Qian et al. [31] utilized physics-informed neural network to predict energy density-based FIP in through silicon via copper; Paulson et al. [14] developed reduced-order models based on spatial statistics and principal component analysis – GNNs have yet to be explored for modeling FIPs.

In this study, we demonstrate the ability of GNNs to model grain-level FIPs as non-linear micromechanical responses of polycrystals under cyclic loading. We show that GNNs can tackle the challenge of modeling FIPs in large MVEs with numerous grains at a modest computational cost. To this end, we trained GNNs using publicly available dataset on Al 7075-T6 alloy [34] featuring CPFE simulation results by Stopka, Yaghoobi et al. [35, 36]. The dataset includes computer-generated

MVEs of various sizes (30^3 to 250^3 voxels, see Figure 1) and grain counts (275 to 160 000) and their simulated micromechanical responses, including spatially-resolved FIPs. For each MVE, we created a microstructure graph whose nodes represent grains and whose edges link adjacent grains, thereby representing grain boundaries. We incorporated different grain properties as node features, including (i) Euler angles and (ii) quaternions – both describing grain orientations – as well as (iii) Schmid factors relative to the loading direction. As a node response for learning and inference, we calculated grain-level Fatemi–Socie FIPs by averaging maximum values from CPFE integration points in a grain. We trained and optimized the GNNs with the three feature choices using a set of 200 smallest MVEs (MVE30) and then tested the trained models on large MVEs. Figure 1 shows a sketch of FIP-GNN, further details of the GNN model, data, training and hyperparameter optimization are described in the Supplementary Material.

We first compare GNNs trained with different node features: Euler angles, quaternions, and Schmid factors. We split the MVE30 set to 180 training and 20 validation MVEs to optimize GNN hyperparameters and evaluate the impact of the feature choice on the GNN performance. All GNNs capture grain-level FIPs with $R^2 > 0.89$ and mean absolute relative error (MeanARE) within 10% (Figure 2). The GNN using Euler angles as features had the lowest accuracy (Figure 2a), while those using quaternions and Schmid factors showed comparably superior accuracy. However, quaternion-

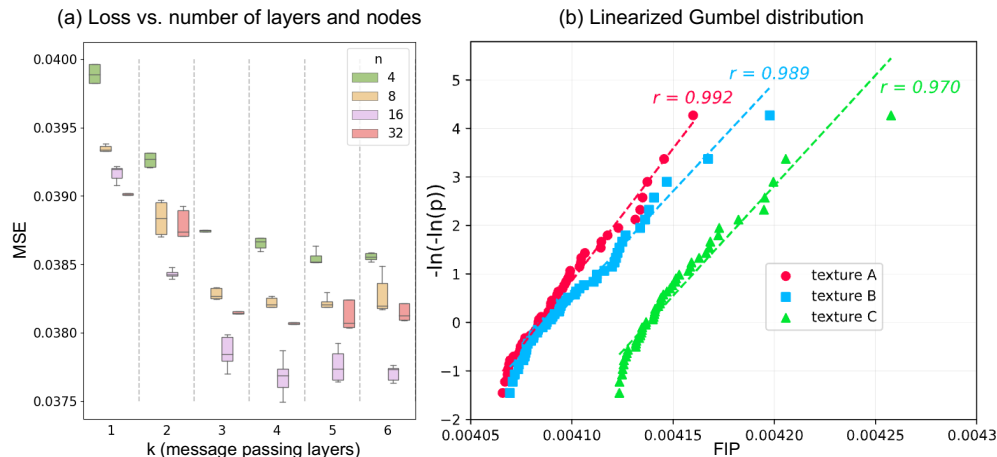


Figure 3: (a) Results of hyperparameter optimization for the GNN model trained with 12 Schmid factors as features shown in terms of the mean squared error (MSE) for a validation set (MVE30-VAL), which was obtained for different combinations of the number of nodes in the hidden layer, n , and the number of message passing layers, k . (b) Gumbel extreme value distribution of FIP values predicted by the optimized GNN for microstructures with three crystallographic textures: cubic texture (A, red circles), nearly uniform texture (B, blue squares), and rolled (C, green triangles), r represents Pearson correlation coefficient of each EV FIP distribution.

based GNN (Figure 2b) required over three times more learnable weights than the Schmid factor-based GNN (Figure 2c) to achieve similar accuracy due to the higher optimal number of hidden layer nodes obtained in hyperparameter optimization (see n in Figure 2b,c). The GNN using Schmid factors also learned fastest reaching validation error plateau in 1000 epochs compared to the 5000 to 6000 epoch range for orientation-based GNNs. Given this combination of accuracy, size, and speed, we focus on GNNs using Schmid factors for the rest of the study.

We next evaluate the GNN’s ability to generalize FIP predictions to large MVEs with grain populations well beyond those used in training. We trained the best GNN identified above with Schmid factors as features and optimized hyperparameters n and k (Figure 3a) on the full MVE30 set and tested its accuracy on MVEs of increasing sizes from 45^3 to 250^3 voxels. Predictions for one MVE from each set show that the GNN accurately predicts grain-level FIPs for large MVEs with significantly larger grain populations than seen during training (Figure 4). The GNN consistently achieves accuracy of $R^2 > 0.96$ for five MVEs representing all studied sizes. Extending this analysis to all MVEs in each set, we summarize the results in a box plot of error distributions (Figure 4f). The difference between GNN-predicted and CPFE values remains

close to zero across all MVE sizes. The error range does not correlate with the MVE size, which again attests to the GNNs ability to predict FIPs for MVEs with large grain populations with consistent accuracy. Finally, FIP fields predicted by the GNN visually match the CPFE fields as shown in representative example MVEs (Figure 4g).

To evaluate the ability of FIP-GNN to efficiently rank microstructures, we analyzed EV distributions of FIP values. We calculated EV distributions for microstructures with three textures distinct from the training set: (A) cubic texture, (B) weak, nearly uniform texture, and (C) rolled texture. Using a public dataset [37] for Al 7075-T6, we compared FIP-GNN predictions with EV distributions and fatigue performance rankings from high-fidelity CPFE simulations. We converted three 90^3 MVEs into graphs, obtained FIPs at each grain with the trained GNN, and extracted 50 highest FIP values for each microstructure. We linearized the distribution of the 50 values using the Gumbel distribution, following prior analyses of FIP EV distributions from CPFE simulations [10, 38]. Figure 3b shows that the 50 highest FIP values predicted by GNN fit the Gumbel distribution (Pearson correlation $r > 0.97$) in all three cases. Furthermore, the GNN-based EV distributions correctly rank the microstructures: texture C performs best and texture A the worst, consistent with CPFE simula-

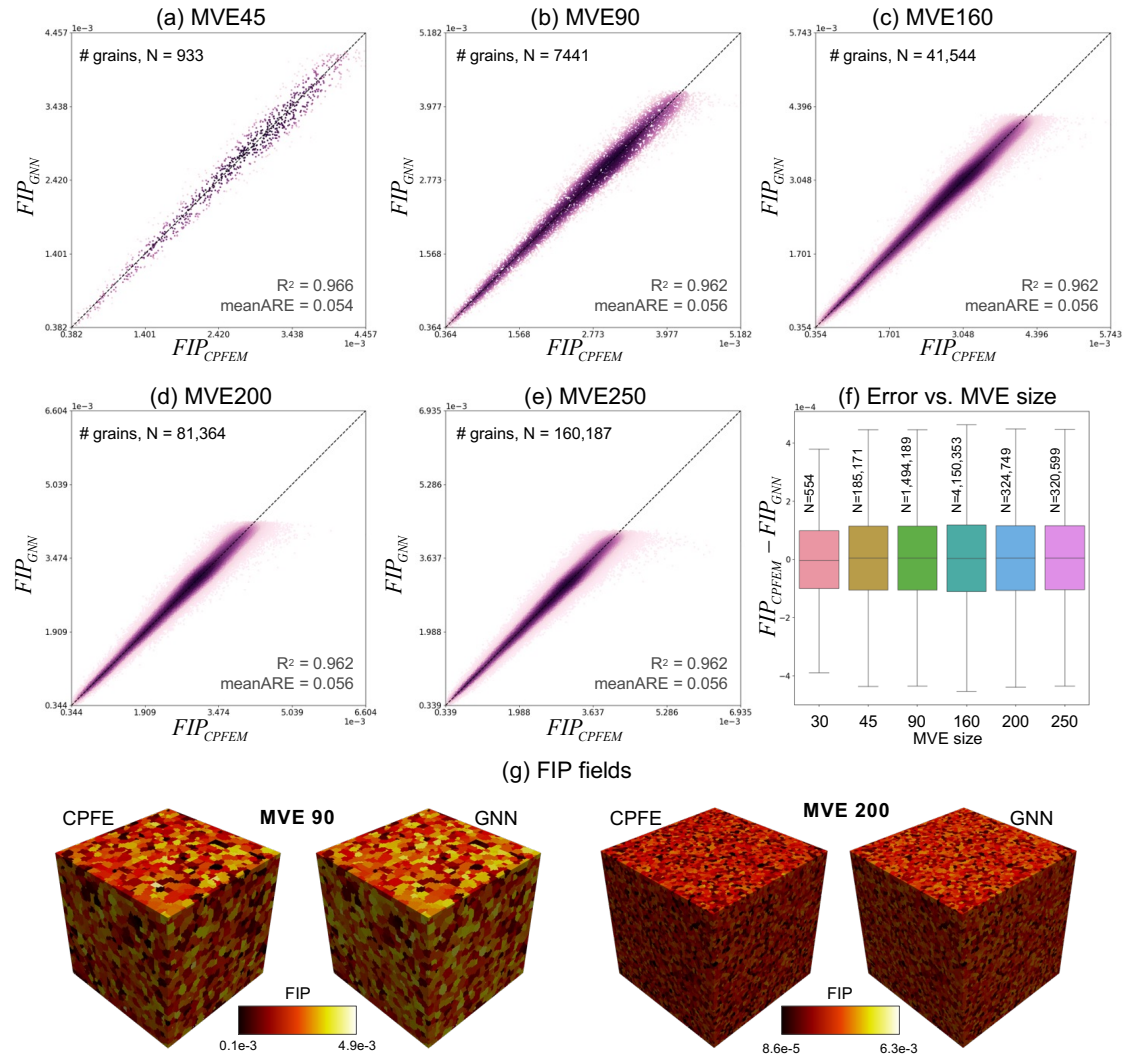


Figure 4: Evaluation of the capability of the GNN trained on 200 microstructures of the MVE30 set to predict FIPs in larger MVEs shown as (a-e) parity plots comparing GNN FIPs with ground truth values from CPFE simulations for individual MVEs of increasing size; (f) box plot showing the distribution of the difference in predicted FIPs from ground truth values; (g) grain-level FIP fields predicted by GNN vs. FIP fields from CPFE simulations.

tions by Stopka et al. [35, 38]. We emphasize that the GNN correctly ranks microstructures with textures distinct from those in the training set, which included only MVEs with uniform textures (i.e., random grain orientations). This analysis confirms the ability of FIP-GNN to capture EV distributions and qualitatively rank individual microstructures in the order consistent with high-fidelity simulations even for microstructures distinct from the training dataset. This is despite some variability in GNN-predicted FIPs at higher magnitudes (Figure 4b-e).

The presented GNN approach enables not only FIP predictions and microstructure ranking but

also insights into micromechanics of polycrystals relevant to FIPs and HCF. Using 12 Schmid factors per grain as node features resulted in the most accurate GNN model (Figure 2) with minimal learnable weights. To explore if all 12 Schmid factors are necessary, we tested a GNN model focusing on Schmid factors of only three most active slip systems per grain. With three highest Schmid factors as features, the GNN model achieved $R^2 = 0.956$ for the MVE30-VAL set. This accuracy is only marginally lower than the full 12-factor model and nearly identical to the quaternion-based GNN (Figure 2b-c). This surprisingly good accuracy of a GNN that

uses only three Schmid factors suggests that the driving force for crack initiation quantified by FIPs is associated with slip activity on very few dominant systems. This is consistent with arguments in literature that few slip systems get activated in each grain during deformation of polycrystals [39]. Further tests showed that even one or two Schmid factors for most active systems still allowed FIP predictions with $R^2 > 0.8$. In addition, the comparable accuracy of the GNN with three Schmid factors and the quaternion-based GNN indicates that Schmid factors provide better accuracy *not* because they offer more features. This clearly follows from the identical accuracy of the GNN with three Schmid factors as three features ($R^2 = 0.956$) compared to the GNN with quaternions as four features ($R^2 = 0.956$). Schmid factors lead to more accurate GNNs at the same or even smaller number of features than orientations can be attributed to more direct relevance to the response of interest (FIPs) and better compatibility with aggregation functions in GNNs [25]. While Schmid factors sufficed in this study of uniaxial cycling of polycrystals, elements of full Schmid tensors (as in [25]) can serve as features for modeling HCF under more complex, multi-axial loading conditions.

We can gain further insight into the role of local microstructure in FIP and crack initiation from the GNN architecture optimized in this study. Our hyperparameter tuning identified the optimal number of message passing layers, k . Each message passing layer aggregates features from the nearest-neighbor nodes in the graph [40] so that stacking k layers aggregates features from neighbors k edges apart. In the context of polycrystal micromechanics, k signifies the range of the local neighborhood that affects the response (FIP) in a given grain. We found $k = 4$ layers optimal for predicting grain-level FIPs (see Figure 3a), meaning Schmid factors up to fourth-order nearest neighbors are necessary for accurate FIP predictions. This data-driven result is consistent with explicit studies of the impact of grain neighborhood on FIPs using physics-based CPFPE simulations. Stopka et al. [35] found that the FIP value in a “hot-spot” grain is sensitive to the orientations of the nearest neighbor grains of up to fourth order for the same alloy studied here. Similarly, our results show that accounting for features from grains beyond four edges away (i.e., $k > 4$) did not improve the accuracy of FIP predictions (Figure 3a).

In conclusion, we developed GNNs for polycrys-

tals that, for the first time (to our knowledge), can (i) predict FIPs as grain-level responses to cyclic loading quantifying the local driving force for crack initiation, and (ii) generalize these predictions to MVEs with grain populations significantly larger than MVEs used in training. These advances contribute to statistically rigorous and computationally efficient modeling of HCF – a long standing challenge in the field. The computational gains of presented GNNs are two-fold: (i) GNNs serve as orders of magnitude faster surrogates to CPFPE simulations of FIPs, and (ii) GNNs can obtain FIPs and their distributions in large MVEs out of reach for direct CPFPE simulations. Indeed, inference with trained FIP-GNN took under 200 ms for the largest MVEs in this study (MVE250) and just 2.5 ms for MVE30 samples on a consumer-grade workstation. In contrast, direct CPFPE simulations of the same FIPs after cyclic loading require over 100 hours for one MVE90 sample on a single CPU [11]. Moreover, unlike CPFPE simulations [41], GNNs exhibit $O(N)$ complexity, meaning their computational cost increases linearly with the number of grains, N , in an MVE. This opens opportunities for rapid calculation of statistically significant FIP EV distributions in microstructures for their ranking in terms of HCF resistance and design for superior HCF life. We confirmed that FIP-GNN can correctly rank microstructures by FIP EV distributions, even for MVEs with textures distinct from those used in training. Finally, we demonstrated that the GNN approach provides insights into the micromechanics of polycrystals during HCF loading consistent with prior physics-based CPFPE modeling.

Code availability

The codes created as part of this study are available on GitHub at <https://github.com/materials-informatics-az/FIP-GNN>.

Acknowledgements

GJS and MGL acknowledge the support from NRF of Korea (grant No. 2022R1A2C2009315) and from the Ministry of Science and ICT (grant No. 2022M317A4072293). The authors thank Dr. Krzysztof Stopka (Purdue University) for help with processing the MVE/FIP dataset used in this study. GJS further thanks Yunju Jang for assistance with some of the illustrations.

Supplementary material

This supplementary material provides the details on the (i) data used for training and testing FIP-GNNs; (ii) microstructure representation with graphs; (iii) GNN architecture design; (iv) GNN training, hyper-parameter tuning, and validation; (v) error metrics.

Data

For training GNNs in this study, we made use of a dataset published by Stopka and Yaghoobi [34], which contains an ensemble of polycrystalline MVEs and the micromechanical data from CPFЕ simulations carried out on these MVEs. The MVEs represent 3D polycrystalline aggregates of an Al 7075-T6 alloy with predominantly equiaxed microstructure and uniform texture [36]. The grain size of the MVEs follows a lognormal distribution with an average equivalent grain diameter of 14 μm and its standard deviation of 2 μm . The crystallographic orientation of each grain in the dataset is described by Euler angles in the ZXZ convention. The dataset contains six subsets of MVEs differentiated by their size that cover a broad spectrum of grain populations. The subsets correspond to six MVE sizes with 30, 45, 90, 160, 200, and 250 voxels along each of the three principal axes. These sizes correspond to the average grain counts per MVE of about 280, 930, 7500, 41 000, 80 000, and 160 000 grains, respectively. We refer to these MVE subsets as MVE30, MVE45, MVE90, MVE160, MVE200, and MVE250, where the number indicates the MVE size in terms of the voxel number in one direction. In terms of the micromechanical data relevant to this study, the dataset includes Socie–Fatemi FIP values calculated with CPFЕ simulations. The simulations captured tension-compression loading of the MVEs along the x axis for two cycles (sufficient for convergence of FIP [35]) and strain amplitude of 0.7% in a completely reversed manner ($R_\varepsilon = -1$). From these simulations, we adopted the grain-average FIP values as the specific grain-level responses to be modeled with GNNs. FIP used in this study is the Fatemi–Socie FIP defined as [10]

$$\text{FIP}_\alpha = \frac{\Delta\gamma_p^\alpha}{2} \left[1 + K \frac{\sigma_n^\alpha}{\sigma_y} \right], \quad (1)$$

where $\Delta\gamma_p^\alpha$ is the range of plastic shear strain and σ_n^α is the maximum normal stress on the α^{th} slip system, K is a parameter quantifying the influence

of normal stress (set to 10), and σ_y is the macroscopic yield strength.

Microstructure graph, node features and response variables

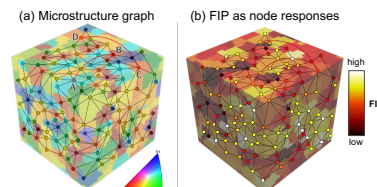


Figure 5: (a) Conversion from MVE to graph. Each grain is represented as a node, and each grain boundary is represented as an edge linking adjacent grains. To account for periodicity of the MVE, node A is ensured to be connected to node B , and node C is connected to node D . (b) Illustration of the assignment of grain-average FIP from CPFЕ fields to graph nodes.

To leverage GNNs for modeling FIPs, we create a microstructure graph for each MVE in the dataset. In the microstructure graph, grains are represented by graph nodes, while grain boundaries are represented by graph edges that link nodes corresponding to spatially adjacent grains (Figure 5a). The MVEs in the dataset are periodic so that the construction of the graphs needs to account for the microstructure periodicity. Specifically, nodes that represent grains on one side of the MVE need to be connected to the nodes representing grain neighbors on the opposite side (A – B and C – D node pairs in Figure 5a for example). Furthermore, when a grain is cut by a side of the MVE and thus its part appears on the opposite side, the grain needs to be represented by a single node in the graph. To satisfy the continuity of the microstructure in the graphs of periodic MVEs, we adopt a simple method that duplicates the given MVE and appends its 26 dummy copies surrounding the original MVE at its six faces, 12 edges and eight corners. Once we have the MVE augmented with dummy copies, we identify grain neighbors using the DREAM.3D software [42]. From the grain neighbor data, we finally construct a graph with the NetworkX library [43].

We then introduce grain-level properties as node features into the constructed microstructure graphs. We tested two orientation representations: (i) Euler angles, and (ii) quaternions. The MVE dataset that we adopted had triplets of Euler angles in radians as the raw orientation data, which

can be readily used as three-element feature vectors. For quaternions as features, we converted the Euler angles into rotation matrices from which we then calculated the four-element quaternion vectors [44]. We further considered Schmid factors of individual grains in respect to the loading direction. Schmid factors quantify resolved shear stresses on each slip system that ultimately drive the dislocation glide in individual grains [45]. For each node in the microstructure graph, we thus assigned 12 Schmid factors calculated for the 12 slip systems in aluminum in respect to the loading direction in the CPFЕ simulations.

In addition to “input” features, we introduced grain-level FIP values as a response variable for inference at each node (Figure 5b). Following the calculation method by Przyblyla et al. [10], we determined the grain-wise FIP by averaging the maximum FIP values over all integration points of each grain. At each integration point, the maximum FIP is found among all slip systems calculated in CPFЕ [34] according to Equation (1). The grain-average FIP values are the node properties modeled by the FIP-GNNs developed in this study.

GNN architecture design, optimization, and training

The GNN architecture considered in this study contained message passing layers and a final output layer as the key components of the architecture. A message passing layer aggregates graph node features from first-order nearest neighbors [46] using an aggregation or convolution function. Stacking k message passing layers results in aggregation of features from k^{th} order neighbors. We considered multiple convolution methods, including SAGE [40], GCN [47], and GIN [48]. Among these methods, SAGE convolution demonstrated significantly better performance in terms of validation error, and was therefore chosen. SAGE convolution includes hidden layers with n neural nodes that process features of each graph node. We treated the number of message passing layers, k , the number of neural nodes in the hidden layer, n , as well as learning parameters (optimizer, rate, decay, number of warm-up steps) as the main hyperparameters that we optimized to our data.

To ensure generalization capability of GNNs to large MVEs, we trained the models and optimized their hyperparameters using only a set of 200 MVEs of the smallest size – MVE30. For hyperparameter optimization, we randomly split the set of 200

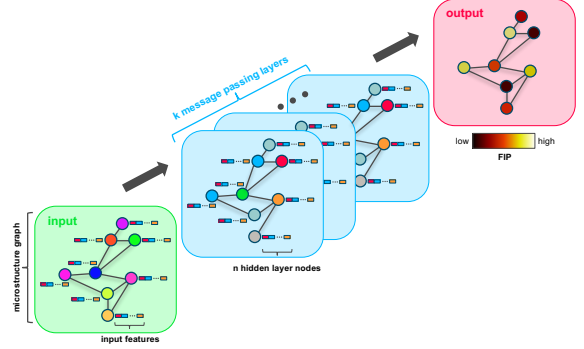


Figure 6: Simplified illustration of the architecture of FIP-GNN comprised including the input graph, k message passing layers (featuring SAGE convolution with n neural nodes in the hidden layer), and output graph with FIPs as node responses.

MVE30 into training (MVE30-TRAIN) and validation (MVE30-VAL) sets in the 90 : 10 ratio. Using validation error as the optimization metric, we found that the convolution method, number of message passing layers, k , and the number of hidden layers, n , had the biggest impact on the GNN training outcome. SAGE convolution was found the best among the tested three methods, while the optimal combinations of the k and n parameters depended on the selected node features (orientations vs. Schmid factors) as summarized in Figure 2 of the main text. Figure 3a in the main text further shows the effect of k and n on the mean squared error for the validation set (MVE30-VAL).

Error metrics

This work uses three error metrics for analysis: mean squared error (MSE), mean absolute relative error (MeanARE), and coefficient of determination (R^2). These metrics are defined as follows.

$$\text{MSE} = \frac{1}{n} \sum_{i=1}^n (y_i - \hat{y}_i)^2, \quad (2a)$$

$$\text{MeanARE} = \frac{1}{n} \sum_{i=1}^n \frac{|y_i - \hat{y}_i|}{|y_i|}, \quad (2b)$$

$$R^2 = 1 - \frac{\sum_{i=1}^n (y_i - \hat{y}_i)^2}{\sum_{i=1}^n (y_i - \bar{y}_i)^2}, \quad (2c)$$

where y_i is the ground truth value, \hat{y}_i is the predicted value, \bar{y}_i is the mean of the ground truth values, and n is the total number of data points.

References

- [1] J. Miao, T. M. Pollock, J. W. Jones, Crystallographic fatigue crack initiation in nickel-based superalloy rené 88dt at elevated temperature, *Acta Materialia* 57 (20) (2009) 5964–5974.
- [2] D. L. McDowell, Basic issues in the mechanics of high cycle metal fatigue, *International Journal of Fracture* 80 (1989) 103–145.
- [3] D. L. McDowell, F. P. Dunne, Microstructure-sensitive computational modeling of fatigue crack formation, *International Journal of Fatigue* 32 (2010) 1521–1542.
- [4] A. Rovinelli, Y. Guilhem, H. Proudhon, R. A. Lebensohn, W. Ludwig, M. D. Sangid, Assessing reliability of fatigue indicator parameters for small crack growth via a probabilistic framework, *Modelling and Simulation in Materials Science and Engineering* 25 (4) (2017) 045010.
- [5] G. I. Barenblatt, On a model of small fatigue cracks, *Engineering Fracture Mechanics* 28 (1987) 623–626.
- [6] F. O. Riemelmoser, R. Pippan, H. P. Stüwe, A comparison of a discrete dislocation model and a continuous description of cyclic crack tip plasticity, *International Journal of Fracture* 85 (1997) 157–168.
- [7] S. T. Rolfe, J. M. Barsom, *Fracture and fatigue control in structures: Applications of fracture mechanics*, ASTM International, 1977.
- [8] A. Fatemi, P. Kurath, Multiaxial fatigue life predictions under the influence of mean-stresses, *Journal of Engineering Materials and Technology* 110 (1988) 380–388.
- [9] G. M. Castelluccio, D. L. McDowell, G. M. Castelluccio, D. L. McDowell, Assessment of small fatigue crack growth driving forces in single crystals with and without slip bands, SpringerGM Castelluccio, DL McDowellInternational journal of fracture, 2012 Springer 176 (2012) 49–64.
- [10] C. P. Przybyla, D. L. McDowell, Microstructure-sensitive extreme value probabilities for high cycle fatigue of ni-base superalloy in100, *International Journal of Plasticity* 26 (2010) 372–394.
- [11] M. Yaghoobi, K. S. Stopka, A. Lakshmanan, V. Sundararaghavan, J. E. Allison, D. L. McDowell, PRISMS-Fatigue computational framework for fatigue analysis in polycrystalline metals and alloys, *npj Computational Materials* 2021 7:1 7 (2021) 1–12.
- [12] T. Gu, K. S. Stopka, C. Xu, D. L. McDowell, Modeling the statistical distribution of fatigue crack formation lifetime in large volumes of polycrystalline microstructures, *Acta Materialia* 247 (2023) 118715.
- [13] M. W. Priddy, N. H. Paulson, S. R. Kalidindi, D. L. McDowell, Strategies for rapid parametric assessment of microstructure-sensitive fatigue for hcp polycrystals, *International Journal of Fatigue* 104 (2017) 231–242.
- [14] N. H. Paulson, M. W. Priddy, D. L. McDowell, S. R. Kalidindi, Data-driven reduced-order models for ranking the high cycle fatigue performance of polycrystalline microstructures, *Materials & Design* 154 (2018) 170–183.
- [15] M. I. Latypov, L. S. Toth, S. R. Kalidindi, Materials knowledge system for nonlinear composites, *Computer Methods in Applied Mechanics and Engineering* 346 (2019) 180–196.
- [16] N. H. Paulson, M. W. Priddy, D. L. McDowell, S. R. Kalidindi, Reduced-order structure-property linkages for polycrystalline microstructures based on 2-point statistics, *Acta Materialia* 129 (2017) 428–438.
- [17] A. Pandey, R. Pokharel, Machine learning based surrogate modeling approach for mapping crystal deformation in three dimensions, *Scripta Materialia* 193 (2021) 1–5.
- [18] O. Ibragimova, A. Brahme, W. Muhammad, D. Connolly, J. Lévesque, K. Inal, A convolutional neural network based crystal plasticity finite element framework to predict localised deformation in metals, *International Journal of Plasticity* 157 (2022) 103374.
- [19] N. N. Vlassis, R. Ma, W. Sun, Geometric deep learning for computational mechanics part i: Anisotropic hyperelasticity, *Computer Methods in Applied Mechanics and Engineering* 371 (2020) 113299.
- [20] D. C. Pagan, C. R. Pash, A. R. Benson, M. P. Kaseimer, Graph neural network modeling of grain-scale anisotropic elastic behavior using simulated and measured microscale data, *npj Computational Materials* 8 (1) (2022) 259.
- [21] E. Sadeghpour, A. Nonn, Data-driven models for structure-property prediction in additively manufactured steels, *Computational Materials Science* 215 (2022) 111782.
- [22] J. M. Hestroffer, M.-A. Charpagne, M. I. Latypov, I. J. Beyerlein, Graph neural networks for efficient learning of mechanical properties of polycrystals, *Computational Materials Science* 217 (2023) 111894.
- [23] A. Thomas, A. R. Durmaz, M. Alam, P. Gumbsch, H. Sack, C. Eberl, Materials fatigue prediction using graph neural networks on microstructure representations, *Scientific Reports* 2023 13:1 13 (2023) 1–16.
- [24] K. Karimi, H. Salmenjoki, K. Mulewska, L. Kurpaska, A. Kosińska, M. J. Alava, S. Papanikolaou, Prediction of steel nanohardness by using graph neural networks on surface polycrystallinity maps, *Scripta Materialia* 234 (2023) 115559.
- [25] G. Hu, M. I. Latypov, AnisoGNN: Graph neural networks generalizing to anisotropic properties of polycrystals, *Computational Materials Science* 243 (2024) 113121. [arXiv:2401.16271](https://arxiv.org/abs/2401.16271).
- [26] M. Dai, M. F. Demirel, Y. Liang, J.-M. Hu, Graph neural networks for an accurate and interpretable prediction of the properties of polycrystalline materials, *npj Computational Materials* 7 (1) (2021) 103.
- [27] Z. Yang, M. J. Buehler, Linking atomic structural defects to mesoscale properties in crystalline solids using graph neural networks, *npj Computational Materials* 2022 8:1 8 (2022) 1–13.
- [28] M. Dai, M. F. Demirel, X. Liu, Y. Liang, J. M. Hu, Graph neural network for predicting the effective properties of polycrystalline materials: A comprehensive analysis, *Computational Materials Science* 230 (2023) 112461.
- [29] Y. Hu, G. Zhou, M.-G. Lee, P. Wu, D. Li, A temporal graph neural network for cross-scale modelling of polycrystals considering microstructure interaction, *International Journal of Plasticity* 179 (2024) 104017.
- [30] C. K. Hansen, G. F. Whelan, J. D. Hochhalter, Interpretable machine learning for microstructure-dependent models of fatigue indicator parameters, *International Journal of Fatigue* 178 (2024) 108019.
- [31] H. Qian, J. Shen, Z. Huang, J. Wang, Q. Zhu, Z. Shen, H. FAN, Stored energy density solution for tsv-cu structure deformation under thermal cyclic loading based

- on pinn, *International Journal of Plasticity* 179 (2024) 104046.
- [32] A. Frankel, K. Tachida, R. Jones, Prediction of the evolution of the stress field of polycrystals undergoing elastic-plastic deformation with a hybrid neural network model, *Machine Learning: Science and Technology* 1 (2020) 035005.
- [33] G. Hu, M. I. Latypov, Learning from 2D: Machine learning of 3D effective properties of heterogeneous materials based on 2d microstructure sections, *Frontiers in Metals and Alloys* 1 (2022) 1100571.
- [34] K. S. Stopka, M. Yaghoobi, [Dataset: PRISMS-Fatigue: predicting distributions of fatigue indicator parameters](#) (2022).
URL <https://materialscommons.org/public/datasets/248>
- [35] K. S. Stopka, M. Yaghoobi, J. E. Allison, D. L. McDowell, Simulated effects of sample size and grain neighborhood on the modeling of extreme value fatigue response, *Acta Materialia* 224 (2022) 117524.
- [36] M. Yaghoobi, K. S. Stopka, D. L. McDowell, L. Graham-Brady, K. Teferra, Effect of sample size on the maximum value distribution of fatigue driving forces in metals and alloys, *International Journal of Fatigue* 176 (2023) 107853.
- [37] Krzysztof S. Stopka, [Prisms-fatigue data - effects of boundary conditions](#) (2021).
URL <https://materialscommons.org/public/datasets/174>
- [38] Effects of boundary conditions on microstructure-sensitive fatigue crystal plasticity analysis, *Integrating Materials and Manufacturing Innovation* 10 (2021) 393–412.
- [39] M. Lee, H. Lim, B. Adams, J. Hirth, R. Wagoner, A dislocation density-based single crystal constitutive equation, *International Journal of Plasticity* 26 (7) (2010) 925–938.
- [40] W. L. Hamilton, R. Ying, J. Leskovec, Inductive representation learning on large graphs, NIPS.
- [41] I. Farmaga, P. Shmigelskyi, P. Spiewak, L. Ciupinski, Evaluation of computational complexity of finite element analysis, in: *2011 11th International Conference The Experience of Designing and Application of CAD Systems in Microelectronics (CADSM)*, 2011, pp. 213–214.
- [42] M. A. Groeber, M. A. Jackson, DREAM.3D: A digital representation environment for the analysis of microstructure in 3D, *Integrating Materials and Manufacturing Innovation* 3 (1) (2014) 56–72.
- [43] A. Hagberg, P. J. Swart, D. A. Schult, Exploring network structure, dynamics, and function using networkx, Tech. rep., Los Alamos National Laboratory (LANL), Los Alamos, NM (United States) (2008).
- [44] D. Rowenhorst, A. Rollett, G. Rohrer, M. Groeber, M. Jackson, P. J. Konijnenberg, M. De Graef, Consistent representations of and conversions between 3D rotations, *Modelling and Simulation in Materials Science and Engineering* 23 (8) (2015) 083501.
- [45] E. Schmid, Beiträge zur physik und metallographie des magnesiums, *Zeitschrift für Elektrochemie und angewandte physikalische Chemie* 37 (8-9) (1931) 447–459.
- [46] J. Gilmer, S. S. Schoenholz, P. F. Riley, O. Vinyals, G. E. Dahl, Neural message passing for quantum chemistry, *CoRR* abs/1704.01212. [arXiv:1704.01212](#).
- [47] T. N. Kipf, M. Welling, Semi-supervised classification with graph convolutional networks, *CoRR* abs/1609.02907. [arXiv:1609.02907](#).
- [48] K. Xu, W. Hu, J. Leskovec, S. Jegelka, How powerful are graph neural networks? (2019). [arXiv:1810.00826](#).